Clays and Clay Minerals, Vol. 49, No. 2, 141–155, 2001.

GENESIS OF DIOCTAHEDRAL PHYLLOSILICATES DURING HYDROTHERMAL ALTERATION OF VOLCANIC ROCKS: II. THE BROADLANDS-OHAAKI HYDROTHERMAL SYSTEM, NEW ZEALAND

YONGHONG YAN,[1] DAVID A. TILLICK,[2] DONALD R. PEACOR,[1] AND STUART F. SIMMONS[3]

[1]Department of Geological Sciences, University of Michigan, Ann Arbor, Michigan 48109, USA
[2]Geology Department, University of Auckland, Private Bag, 92019, Auckland, New Zealand
[3]Geothermal Institute, University of Auckland, Private Bag, 92019, Auckland, New Zealand

Abstract—The clay mineral textures, assemblages, formation mechanisms, and controlling geological parameters relating to alteration of silicic volcanic rocks by hydrothermal solutions, in core samples from the Broadlands-Ohaaki hydrothermal system, New Zealand, were investigated using X-ray diffraction (XRD), scanning electron microscopy (SEM), and transmission and analytical electron microscopy (TEM/AEM). Mineralogical and textural relations of this active hydrothermal system, for which temperatures and fluid relations are well known, are equivalent to those in the Golden Cross hydrothermal gold deposit as described in Part 1.

XRD data show a sequence of clay minerals from smectite to a range of interstratified I–S to mica with increasing depth and temperature, on average. TEM observations are in general agreement with XRD data, especially with respect to relative proportions of illite (I)- and smectite (S)- like layers. TEM data also show that: (1) Smectite packets contain no discrete illite-like layers in samples identified as (Reichweite, R = 0) I–S by XRD. They coexist with separate packets of (R = 1) I–S. (2) A continuous range in I–S occurs from (R = 1) I–S with increasing proportion of illite-like layers, but at high illite-like layer contents there is a gap between I–S and illite. (3) $1M$ and $2M_1$ polytypes of mica coexist in separate packets, but the rare $1M$ polytype has a larger ^{VI}Mg content.

The data imply that clay minerals formed by dissolution and neocrystallization directly from volcanic phases, although multiple reaction events can not be ruled out. Such "episodic" alteration produces a sequence of clay minerals identical to those of prograde diagenesis of pelitic sediments. This result implies that the presence of a continuous sequence is not definitive proof of continuous sequences of transformation as a function of time and continuous burial. Reaction progress of the clay-mineral sequence is in general accord with the known temperature gradient, but with significant and common exceptions. High porosity and permeability, both inherent in rock texture and local structure, are inferred to foster local reaction progress, as consistent with metastability of phases and the Ostwald step rule.

Key Words—Crystallization, Dioctahedral Phyllosilicates, Hydrothermal System, Illite-Smectite (I–S), Polytypism, Transmission Electron Microscopy.

INTRODUCTION

The Broadlands-Ohaaki geothermal system, North Island, New Zealand, is a currently active geothermal system. The geological relations of this system have been well studied (Simmons and Browne, 2000, and references therein). In our study, X-ray diffraction (XRD) and transmission electron microscope (TEM) techniques were used to characterize hydrothermal clays in the Broadlands-Ohaaki geothermal system to determine the characteristics of interstratified illite-smectite (I–S), the textural relationships among the dioctahedral clay minerals, and the mechanism(s) of clay formation. The system is hosted by volcanic rocks and contains a dioctahedral clay-mineral series from smectite through I–S to muscovite, similar to that found in sedimentary sequences such as the Texas Gulf Coast shales. A unique opportunity exists to correlate temperature, fluid composition, and other variables with the assemblages of clay minerals for comparison with ancient systems, such as the Golden Cross gold-silver epithermal deposit (Tillick *et al.*, 2001). This is the second of a two-part series, the first being a description of the clay mineral relations at the Golden Cross mine. Because this study was integrated with Part I, the introduction in Tillick *et al.* serves as an introduction to the integrated results, and the reader is referred to that paper for further introductory material. We note here that although the observations and conclusions of the two studies are similar, conclusions by Tillick *et al.* emphasize formation mechanisms, whereas the clay mineralogical relations are emphasized herein. The conclusions of both papers are dependent on the closely related observations of both studies, however.

THE BROADLANDS-OHAAKI GEOTHERMAL SYSTEM

The Broadlands-Ohaaki hydrothermal system is located on the east side of the Taupo Volcanic Zone (TVZ) and is one of ~20 known hydrothermal systems in the region (Figure 1). It is characterized by widespread volcanism and hydrothermal activity resulting from crustal extension and anomalous heat flow in a

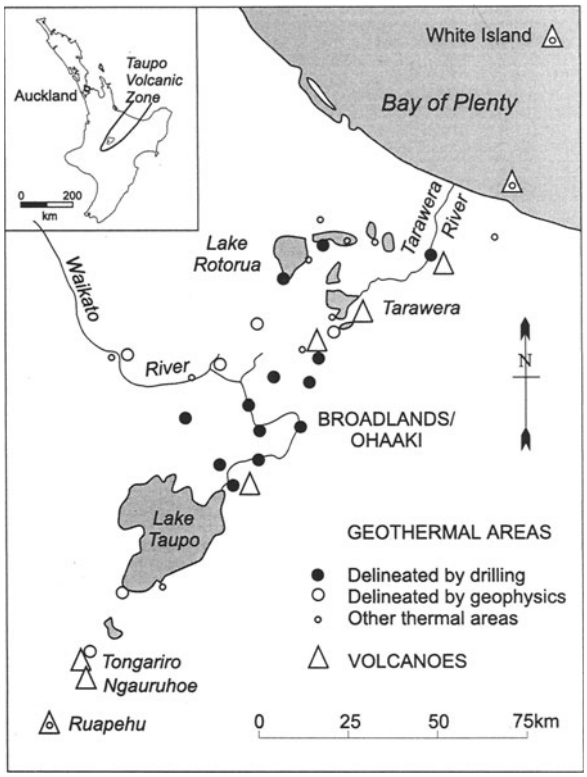

Figure 1. Map showing the location of the Broadlands-Ohaaki hydrothermal system in the Taupo Volcanic Zone (TVZ) of the North Island, New Zealand.

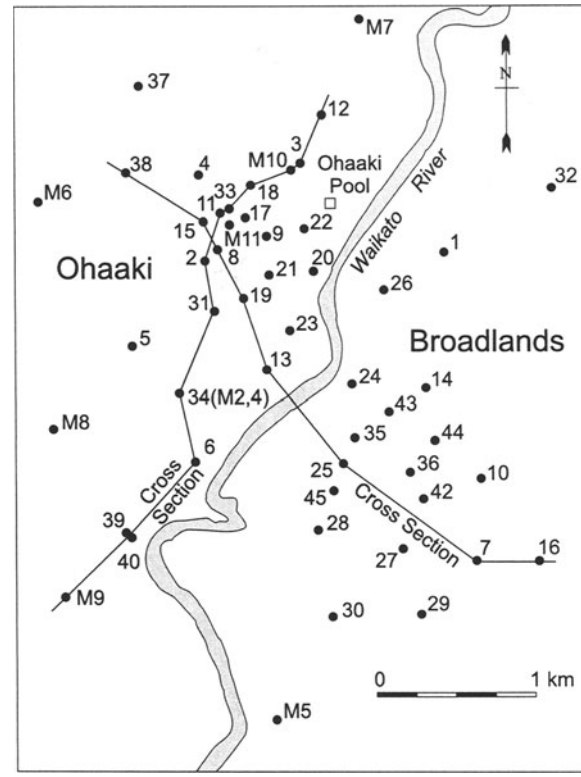

Figure 2. Plan-view of the Broadlands-Ohaaki fields, showing the locations of wells used to construct cross-sections.

complex volcanic arc setting. These systems have large water/rock ratios and involve large-scale convection of meteoric water driven by heat flow derived from magmatic intrusions at depth. Overviews of their features are given by Hedenquist (1986), Henley *et al.* (1986), and Simmons *et al.* (1992). Drilling at Broadlands-Ohaaki resulted in 52 vertical wells ranging in depth from ~370 to 2600 m. The long lead-in time to commissioning the 112-MW electrical power station in 1989 resulted in a number of research papers on the physical and chemical nature of the system in a nearly undisturbed state, as summarized by Hedenquist (1990) and Simmons and Browne (2000). Grindley and Browne (1968) described the subsurface geology, whereas Hedenquist (1990) described the fluid chemistry and hydrology.

Wells penetrated a layered sequence (Quaternary to Recent) of rhyolitic to dacitic tuffs, tuff breccias, and lavas (total thickness 800 to >2000 m) underlain by a block-faulted, Mesozoic graywacke basement, with well locations shown in Figure 2. Maximum temperatures within the upflow zone are controlled by the hydrostatic boiling point for a given depth. Permeability in most of the system is controlled by rock type and fractures. Fractures are generally discontinuous and narrow (<1 cm width) as documented in drill cores and by circulation losses during drilling.

Optical microscopy and XRD were used to determine the occurrence, distribution and abundance of dioctahedral clays in >500 core samples obtained during exploratory drilling (Browne and Ellis, 1970; Browne, 1971; Simmons and Browne, 2000). Interstratified I–S is the most abundant clay mineral, comprising <70% of the altered volcanic rock. Clay-mineral abundance generally increases upwards and towards the margin of the upflow zone, but decreases toward the periphery of the system. Illite, I–S, and smectite commonly replace feldspars, ferromagnesian minerals, and volcanic glass. Smectite is common at shallow depths and on the periphery, occurring in slightly altered glassy volcanic rocks, and in very fine-grained lake sediments that occur at shallow depth (<500 m). Smectite gives way to illite with increasing temperature. This transition is marked in many places by irregularly shaped zones (0 to >200 m thick) of interstratified I–S (Figure 3). The XRD data imply that interstratified I–S with 60–100% expandable layers displays random interstratification (R = 0), whereas I–S with 0–50% expandable layers has ordered interstratifications (R = 1, R = 2, and R ≥ 3). Aqueous log a_{Na^+}/a_{K^+} values of activities (a) range from 0.75 to 1.75, well within the stability field of potassium-bear-

https://doi.org/10.1346/CCMN.2001.0490204 Published online by Cambridge University Press

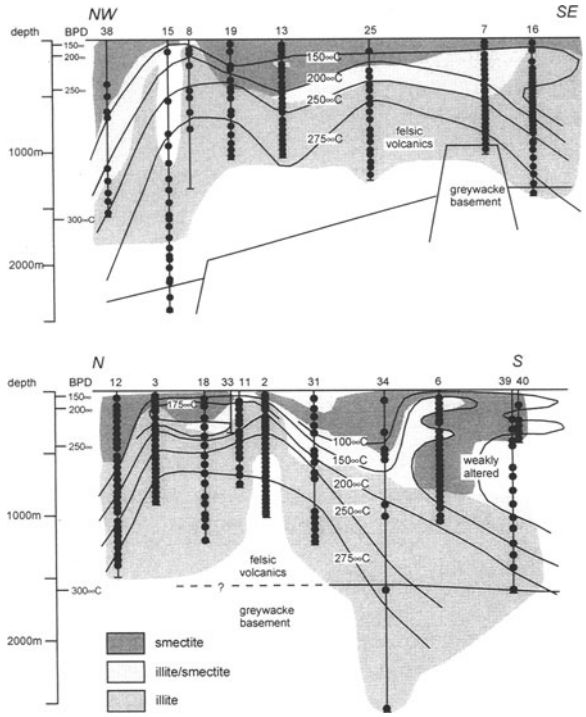

Figure 3. Cross-sections through the Broadlands-Ohaaki geothermal system showing subsurface temperature gradients and distribution of clays (after Simmons and Browne, 2000).

ing aluminosilicates, given values of $a_{SiO_{2(aq)}}$. The weakly acidic nature of the deeply derived and peripheral CO_2-rich thermal waters, with log a_{K^+}/a_{H^+} between 2.7–4.0, favors the formation of clay minerals (*i.e.*, K-rich mica) over K-rich feldspar, except in the shallower parts of boiling zones.

SAMPLE DESCRIPTIONS

This study focuses on the interstratified clays that occur in the Broadlands dacite in well Br7 (Figure 2). This is the longest vertical interval of interstratified I–S at Broadlands-Ohaaki, and it is restricted to a single rock unit. There is a well-defined general trend of increasing temperature and increasing proportion of non-expandable layers in clays, with increasing depth. That general sequence is shown by well Br7, but with reversals in the proportions of non-expandable clay layers (Table 1; Figure 2); that is, the proportion of illite-like layers decreases with increasing depth for some samples. Samples were chosen in part because such inconsistencies with the overall trend may provide insight to the parameters causing variations in clay minerals. Subsequent scanning electron microscopy (SEM) and TEM observations showed that even the deepest samples in well Br7 did not contain the illite or muscovite typical of the highest grade and deepest samples of other wells. Sample Br1842 from well Br16, which is adjacent to well Br7 (Figure 2), was chosen to represent the higher grade material.

Broadlands dacite is an "informal" stratigraphic name for the lithology encountered in 14 geothermal wells of the Broadlands-Ohaaki geothermal system. This unit does not crop out on the surface but was intersected by wells in the central and southeastern parts of the system, attaining its greatest thickness (>450 m) in wells Br7 (142–632 m depth) and Br16 (164–631 m depth). Petrographic descriptions of this unit are reported by Browne and Ellis (1970) and Browne (1973). Least-altered cores are hard, dense, dark-gray to black; the unit is variably brecciated. Primary minerals are dominated by euhedral crystals of zoned andesine, whereas uncommon pyroxene and amphibole phenocrysts were replaced largely by chlorite; fine-grained subparallel laths of plagioclase comprise the groundmass. Unaltered plagioclase and the low abundance of clay (<10%) in Br7 between 274–518 m correspond with poor permeability (Browne and Ellis, 1970; Browne, 1973). Quartz, illite, I–S, smectite, calcite, pyrite, and chlorite are the abundant secondary minerals (Table 1), with the distributions of dioctahedral clay minerals being shown in Figure 3. The abundance of hydrothermal clay ranges from 20 to ~50% in the shallow (142–274 m depth) and deep (518–632 m depth) samples in Br7 cores from this unit

Table 1. Summary description of six Broadlands-Ohaaki samples in this study. The data for alteration mineralogy are from Browne (1971). Depth in feet is below Kelly Drive.

Sample number	Well-depth[2] (ft./m)	Temp. (°C)	%Illite	Reichweite value	Lithology	Alteration minerals
Br533	7-533/162	150 ± 10	75	R = 1	Brecciated Dacite	I-S, Py[1], Cal
Br693	7-693/208	165 ± 10	60	R = 1	Dacite	Qtz, Chl, I-S, Py
Br836	7-836/254	170 ± 5	55	R = 1	Brecciated Dacite	Chl, I-S, Py
Br1270	7-1270/387	195 ± 10	<10	R = 0	Hard Dense Dacite	I-S, Chl, Leu, Py, Cal, Qtz
Br1702	7-1702/517	245 ± 10	50	R = 1	Dacite	Cal, I-S, Qtz, Leu, Chl, Py
Br1842	16-1842/558	130 ± 10	100	n.a.[3]	Brecciated Dacite	Qtz, Ill, Py, Chl, Leu, Cal, Ad, Sp, Gn

[1] Abbreviations: Ad = adularia, Cal = calcite, Chl = chlorite, Gn = galena, Ill = illite, I-S = illite-smectite, Leu = leucoxene, Py = pyite, Qtz = quartz, Sp = sphalerite (Browne, 1971).

[2] Depth in meters is measured from the surface, depth in feet is measured from Kelly Drive.

[3] n.a. = not applicable. This sample is comprised of mica.

https://doi.org/10.1346/CCMN.2001.0490204 Published online by Cambridge University Press

(Browne, 1969). Veins, which are more abundant than in other formations, are the main host for base-metal sulfide minerals (Browne, 1969, 1971).

Steam-heated water currently fills the pore spaces and fractures near wells Br7 and Br16 as determined from the down-hole composition of fluids leaking into the wells through casing breaks caused by corrosion (Hedenquist and Stewart, 1985). The presence of the water is consistent with the abundance of hydrothermal clay and calcite, and the isotopic compositions of calcite in the altered rocks (Hedenquist, 1990; Simmons and Christenson, 1994). Alteration mineral assemblages and fluid inclusion data from well Br16 indicated the former existence of boiling temperatures, however, implying that the present temperatures caused by steam-heated water were preceded by higher temperatures (Simmons and Browne, 1997). Thus sample Br1842 (well Br16) shows a measured well temperature of ~130°C, although the host mineral assemblage and stable-isotope data suggest deep formation-water temperatures >200°C (Eslinger and Savin, 1973; Simmons and Browne, 2000). In Br7, comparison of fluid inclusion data from 845 to 896 m depth and well measurements show that temperatures in this interval have declined from ~280–290 to 265–270°C (Hedenquist, 1990). Despite this, there is no mineralogical evidence of chemical or thermal overprinting within the Broadlands Dacite (Browne and Ellis, 1970). Accordingly, we assume that the modern normal temperature gradient (*i.e.,* one that increases with depth) has existed throughout the period of hydrothermal activity and clay formation, but that temperatures may have cooled during this period by <20–25°C.

EXPERIMENTAL METHODS AND NOMENCLATURE

Methods

Powder XRD data were obtained for air-dried and ethylene-glycol treated samples of oriented clay separates and powdered bulk rock. Oriented separates were obtained by gently crushing samples with a mortar and pestle and then dispersing them in a water slurry with a blender for 5 min. The <2.0-μm fractions were obtained by gravity settling and centrifuging; they were then mounted on glass slides. Air-dried XRD data for bulk samples were obtained with a Philips automated diffractometer with a graphite monochromator and CuKα radiation (35 kV and 15 mA), using a step size of 0.020°2θ, counting time of 10 s/step and scanning range from 2 to 32°2θ. Data for oriented separates were determined by using a Philips 1050/25 diffractometer with CuKα radiation (40 kV and 20 mA) and a graphite monochromater. Methods of preparation of samples for SEM and TEM observations, as well as conditions and methods of observation, were described by Tillick *et al.* (2001). Analytical electron microscopy (AEM) analyses were obtained by rastering over areas as large as possible, in part to minimize alkali diffusion. Areas analyzed were first characterized by TEM observations to verify that they corresponded to single minerals or single varieties of interstratified layers.

Nomenclature

Individual I–S units as observed in TEM lattice-fringe images are described following Bauluz *et al.* (2000). This nomenclature is based on the Reichweite nomenclature, but uses direct observations of specific layers, rather than for averaged material as observed by XRD. Thus, individual units of I–S (*e.g.,* IS, IIS, IIIS) observed by TEM are reported as I*n* units, where *n* is the number of illite-like layers (*e.g.,* I1, I2, I3, respectively). This is especially useful for large numbers of illite-like layers and serves to discriminate between XRD and TEM results.

A 2:1 phyllosilicate was observed by TEM in the highest grade samples which is like muscovite and unlike illite in having a stacking sequence of an ordered polytype ($2M_1$ or $1M$), but with some stacking disorder. However, the phase is deficient in interlayer cations (*i.e.,* like illite and unlike muscovite). Because it shares characteristics, as observed by TEM, of illite and muscovite, and it appears to be transitional to these phyllosilicates, we refer to it as "mica" for the purposes of this paper. Lower grade samples have an interlayer-cation deficient, non-expandable 2:1 phyllosilicate with $1M_d$ stacking. These are the characteristics, as observed by TEM, of illite, and we refer to that material as illite.

RESULTS

XRD data

XRD patterns of all bulk samples confirmed that the principal clay minerals are smectite, I–S, illite or mica, and chlorite, whereas other secondary hydrothermal minerals are K-rich feldspar, albite, pyrite, calcite, and quartz (Table 1). XRD patterns of <2-μm, ethylene-glycol solvated, clay-separates are shown in Figure 4. Data obtained from XRD patterns are listed in Table 1 and plotted in Figure 5. Figure 5a shows the percentage of illite-like layers in I–S and Reichweite (R) values obtained from values for 001/002 and 002/003 peaks according to the method of Inoue and Utada (1983), whereas Figure 5b is a plot of measured well temperature *versus* % illite layers. Data are shown only for samples studied by TEM, but they are representative of a much larger set of XRD data as indicated in Figure 3 (Simmons and Browne, 2000).

Petrographic and SEM observations

Observation of thin sections by petrographic microscope shows that the six samples chosen for TEM ob-

https://doi.org/10.1346/CCMN.2001.0490204 Published online by Cambridge University Press

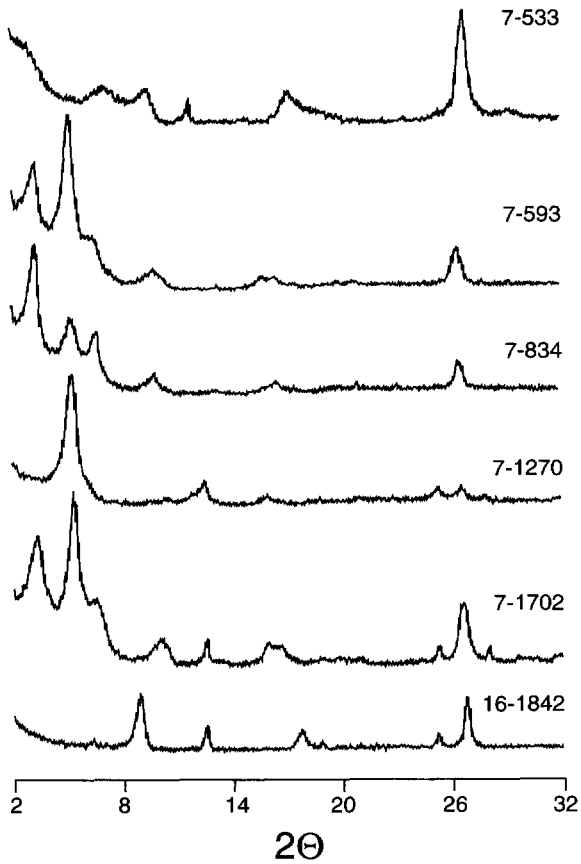

Figure 4. XRD patterns of ethylene-glycol solvated, <2-μm separates of samples studied by TEM.

servations appear similar. They are generally homogeneous at the optical scale, without obvious contrast owing to features such as phenocrysts or pores lined with clay minerals. Back-scattered electron (BSE) images of two samples, Br836 and Br1842, represent the two principal textures observed by SEM (Figure 6). These images were obtained from surfaces which were ion-milled, as such surfaces produce images of the highest quality. Sample Br1842 consists mostly of small areas with light contrast, but contrast varies locally from light to dark (Figure 6a). TEM images (see below) showed that those areas are composed mostly of clay minerals. Energy dispersive spectrum (EDS) analyses with the SEM did not correspond to a single phase, but involved mixtures of clay minerals and quartz at the level of resolution of the instrument, ~1 μm, as consistent with variable image contrast. The other principal kind of texture, shown in the lower right area of Figure 6a, consists of brecciated fragments in a fine-grained matrix of materials which cannot be resolved. The matrix gives EDS analyses consistent with a high proportion of clay minerals. Sample Br836 is typical of the brecciated kind (Figure 6b). The fine-grained matrix is dominated by clay minerals; it is the specific material studied subsequently in detail by TEM, and described below. Minerals identified by EDS analyses, with sizes sufficiently large to be resolved in the SEM, include quartz, feldspars, pyrite, calcite, dolomite(?), and Ti and Fe-oxides; the clay minerals were dominated by dioctahedral clays, but trioctahedral clays also were commonly observed.

Low-resolution TEM observations

To visualize the textural relations and significance of the clay minerals shown in high-resolution TEM images (below), textural features are described at a scale of low-resolution TEM here. Consistent with the relative homogeneity of texture observed petrographically and in BSE images, low-resolution TEM images of all samples are similar, and illustrated by Figure 7. Figure 7a is typical of images of smectite and I–S, as

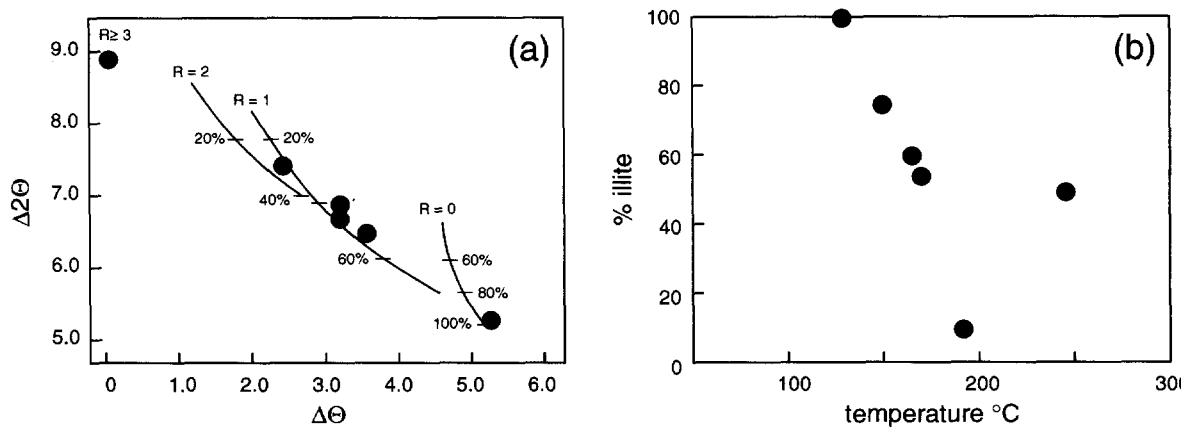

Figure 5. Data from XRD analyses of oriented clay mounts for samples from wells Br7 and Br16 which were chosen for TEM observation. a) Plot of $\Delta 2\theta_1$ and $\Delta 2\theta_2$, following the method of Inoue and Utada (1983). Percentages refer to the amount of smectite. b) Plot of percentage of illite in I-S *vs.* temperature measured in wells.

https://doi.org/10.1346/CCMN.2001.0490204 Published online by Cambridge University Press

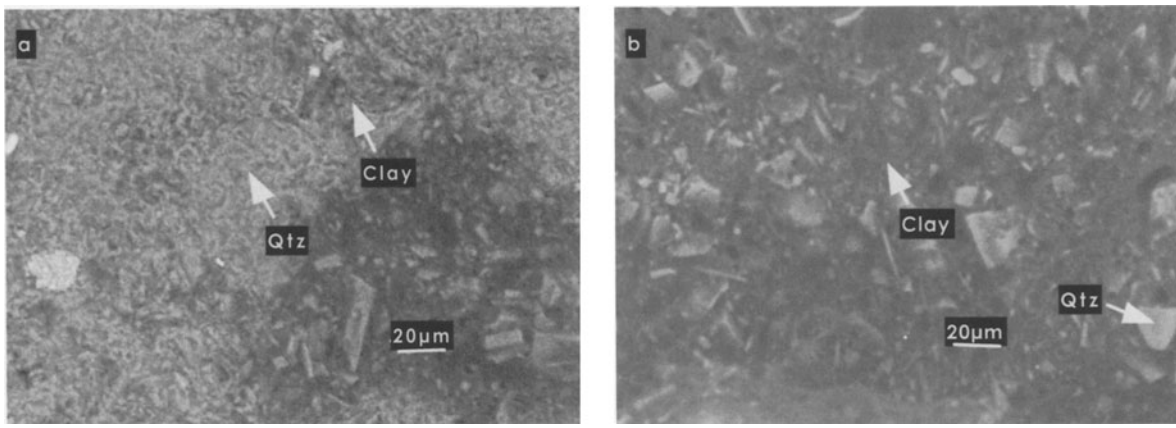

Figure 6. Representative SEM-BSE images of samples Br1842 and Br836. (a) Br1842 consists of two kinds of texture: fine-grained clay minerals in areas with light, but irregular contrast, and brecciated fragments in a fine-grained matrix rich in clay minerals. (b) Br836 consists entirely of the brecciated kind, with clay minerals dominant in the fine-grained matrix.

illustrated for sample Br836, for which XRD identified the clay as consisting of (R = 1) I–S, with 55% illite-like layers. The I–S occurs in packets ~500 Å in width and ~5000 Å in length. Although boundaries are sharply defined along (001) surfaces, they have feathery terminations. Curvature of packets is common. More than one packet appears to diverge from a common origin, thickening away from the common apex. Packets are randomly oriented, as commonly observed where crystallization occurred in a stress-free environment. Pore space is abundant. Proportion can not be measured precisely, in part because three-dimensional

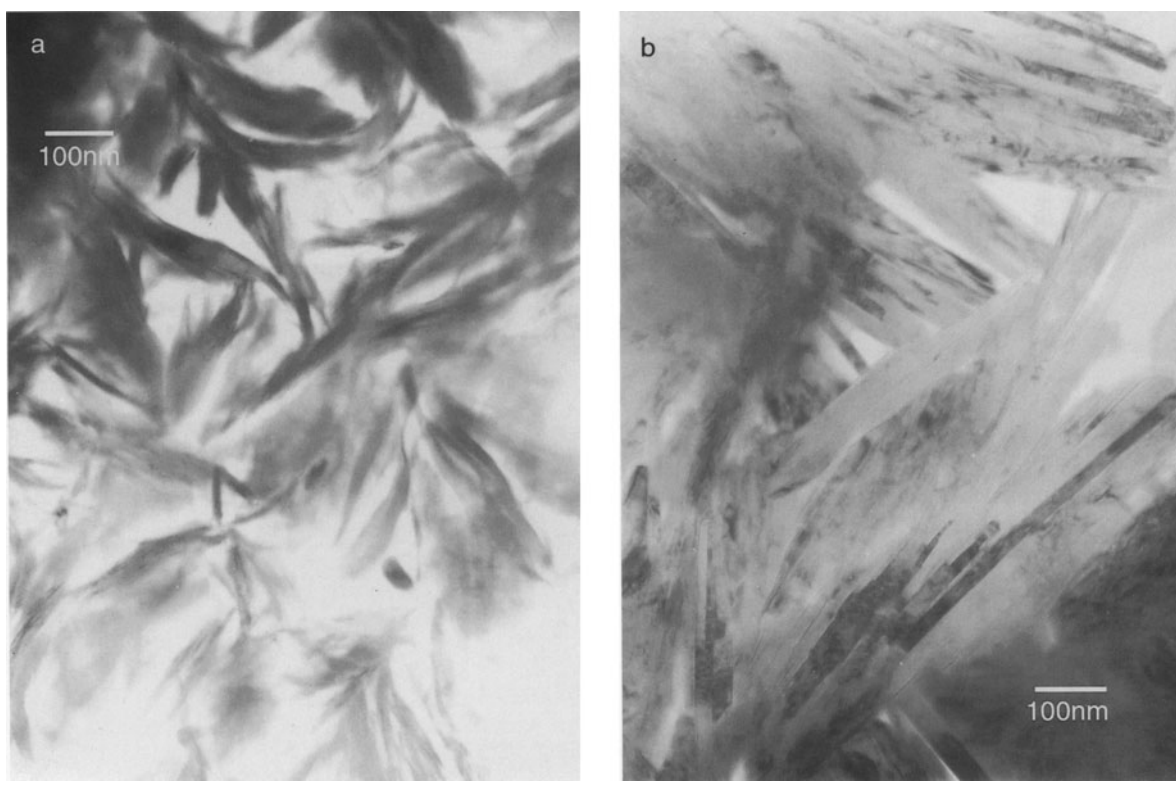

Figure 7. Low-resolution TEM images of samples Br836 and Br1842. (a) I-S in sample Br836. This image is typical of all samples of smectite and I-S. Packets are randomly oriented and have curved boundaries which thicken away from apices common to more than one packet. Pore space is abundant. (b) Mica in sample Br1842. Straight packets of mica ~300 Å thick comprise stacks or transect pore space.

https://doi.org/10.1346/CCMN.2001.0490204 Published online by Cambridge University Press

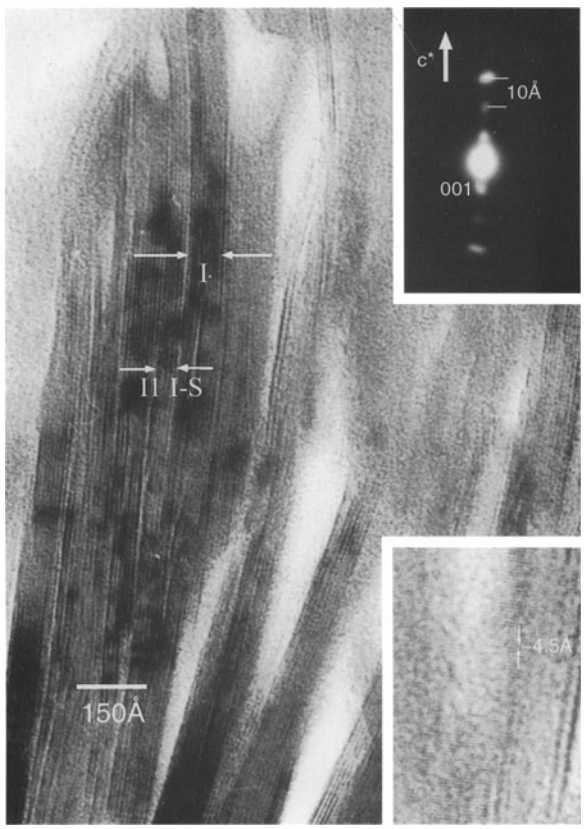

Figure 8. High-resolution TEM lattice-fringe image of sample Br533. Most packets are comprised of illite layers, with straight fringes with 10-Å spacing and uniform contrast I1 I-S (21–22 Å periodicity) also occurs, but not as single random layers within illite. Cross fringes with a spacing of 4.5 Å range across six to ten layers, as shown by the lower inset. The upper, inset SAED pattern is typical of illite.

relations are projected onto the image surface, but pore spaces appear to constitute <25% of the sample volume. This material is similar to smectite which is commonly observed to directly replace volcanic glass (*e.g.,* Masuda *et al.,* 1996), and where replacement has been directly observed as transitional between presently existing glass and smectite.

Figure 7b is of material of higher metamorphic grade, with packets comprised only of illite or mica. Packets are straight, have sharp boundaries commonly defined by a single, continuous (001) layer, and range in thickness from 300 to 600 Å. Subparallel packets commonly form thick stacks. Some individual packets cut across pore space, defining a texture which is in sharp contrast to that relating to direct replacement. Such textures, in which subhedral to euhedral crystals occupy void space that was occupied by fluids, probably relate to direct crystallization from a pore fluid, as in the Salton Sea area (Yau *et al.,* 1987). There is no apparent preferred orientation. Although pore space is limited (Figure 7b), other images show abundant pore space, with a high proportion of individual crystals, *i.e.,* not occurring in stacks.

High-resolution TEM images

Sample Br533 (75% I in I–S, by XRD). Figure 8 is a lattice-fringe image showing clay minerals occurring in parallel to sub-parallel packets of relatively small numbers of layers. The majority of fringes have constant contrast and 10-Å spacing characteristic of illite. The illite was verified by selected area electron diffraction (SAED) patterns indicating $1M_d$ stacking, and AEM analyses. Fringes for smectite- and illite-like layers in interstratified I–S are characterized by: (1) differences in contrast (Guthrie and Veblen, 1989; Veblen *et al.,* 1990); *e.g.,* (R = 1) I–S (50% I) shows fringes that are alternately light and dark, and (2) differences in spacing. For samples treated with L.R. White resin, Dong *et al.* (1997) showed that smectite gives spacings of 12–13 Å, I1 I–S has periodicity of ~21 Å, I2 I–S ~31 Å, *etc.*; the excess over values of multiples of ten are probably related to the thicker smectite-like interlayer. Observations of these parameters in images of sample Br533 (*e.g.,* Figure 8) demonstrate that most packets are comprised only of illite layers. However, fringe contrast and spacings of some sequences are of the I1 type, where smectite-like layers occur within I1 I–S layer sequences, rather than as layers randomly intercalated in sequences dominated by illite-like layers (although such intercalation was also observed). The sequences of layers thus consist of dominant illite, but with associated thin I1 I–S packets.

The fringes are relatively straight, in contrast to those of smectite. Layer terminations (edge dislocations) are relatively uncommon. More importantly, cross fringes with spacings of 4.5 Å were observed ranging across as many as six to ten sequential layers, as illustrated in Figure 8 (lower inset). They transect smectite fringes as well as illite-like fringes. Such cross fringes have been inferred to demonstrate coherency across interlayers (*e.g.,* Peacor, 1998), although Guthrie and Reynolds (1998) concluded that they may reflect semicoherency. The inset SAED pattern is typical of a relatively disordered stacking sequence ($1M_d$ polytypism), in that non-00*l* reflections are diffuse and non-periodic.

Sample Br693 [(R = 1) I–S, 60% I]. Lattice-fringe images show that I1 I–S is the dominant phase. Figure 9 illustrates typical material, with fringes showing the alternating contrast with dominant spacing of 21–22 Å; the sequence of layers is almost entirely of I1 with only rare occurrences of other sequences such as I2. Other lattice-fringe images (not shown) show small numbers of fringes lacking alternating contrast, and with spacings of 12–13 Å. Sequences were comprised of only three or four such adjacent layers. This ma-

https://doi.org/10.1346/CCMN.2001.0490204 Published online by Cambridge University Press

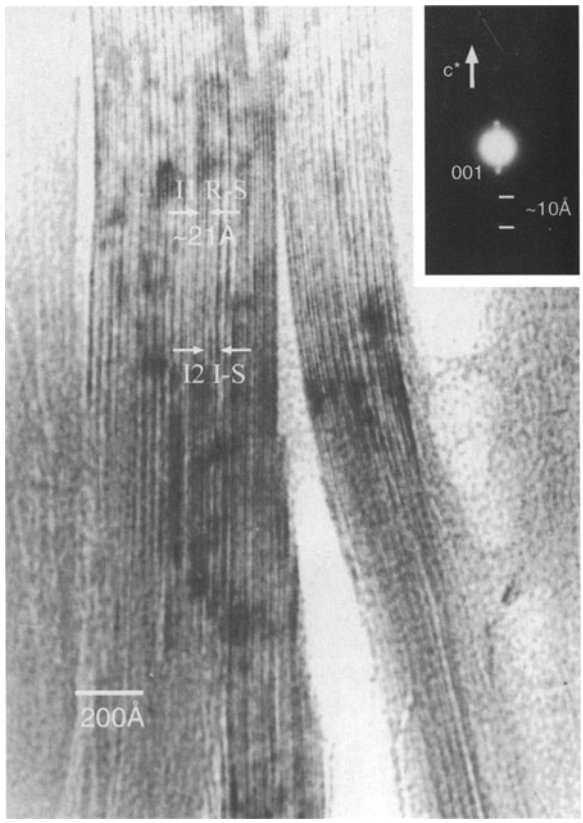

Figure 9. High-resolution TEM lattice-fringe image of sample Br693. I1 I-S units dominate the layer sequences, with fringes alternating in contrast and having periodicity of 21–22 Å. Two or three fringes of smectite occur together. The SAED pattern shows rare, weak 001 reflections with 21-Å periodicity, in addition to the strong reflections of the 10-Å pattern.

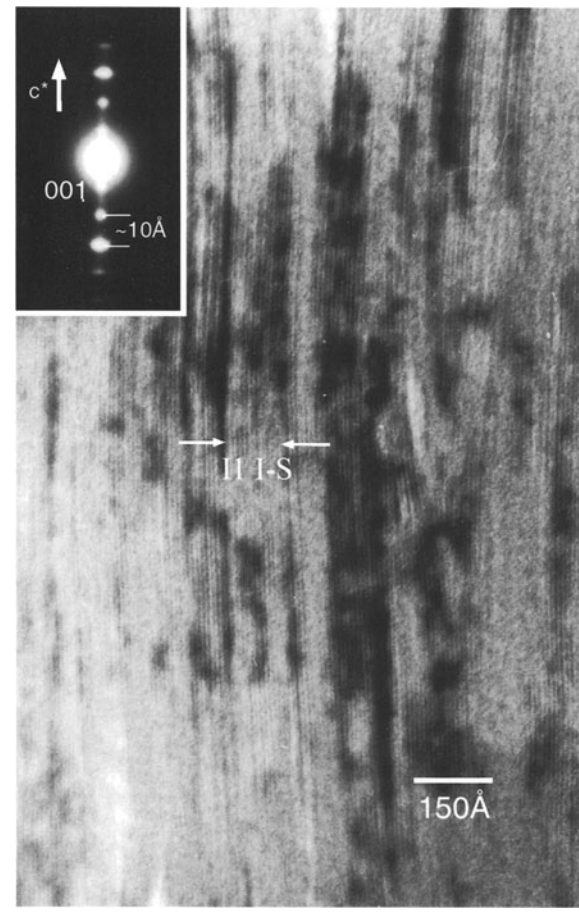

Figure 10. High-resolution TEM lattice-fringe image of sample Br836. I1 units dominate the sequence, but some I2 and less-common I3 units occur randomly. The inset SAED pattern shows the 00*l* reflections with 10-Å periodicity typical of I-S.

terial is smectite. The collective lattice-fringe images of this sample therefore are consistent with dominant I1 I–S and subordinate smectite. The proportions of illite-like and smectite-like layers are qualitatively consistent with the XRD data, but inconsistent with the implied interlayer relations.

The SAED patterns are unusual, in that the 003 reflection corresponding to 21-Å I1 periodicity was observed, although very weakly. Normally, only orders of 10-Å reflections are detected. In most images of I–S, however, there are significant numbers of units such as IIS; such units perturb the IS sequence, and thus cause weakening of reflections such as 003. The occurrence of 003 is thus a measure of the relative perfection of the IS layer sequence. The non-001 reflections show the diffuseness and non-periodicity typical of $1M_d$ polytypism combined with turbostratic stacking in a given stack of layers.

Sample Br836 [(R = 1) I–S, 55% I]. Figure 10 shows a representative lattice fringe image. The dominant layer sequence is I1, but units such as I2 and, less commonly, I3 also occur, randomly interspersed with I1 units. No separate smectite or illite packets were observed. Cross-fringes were occasionally observed, transecting ~5 smectite-like layers, on average. The 00*l* sequences of reflections in SAED patterns corresponded to 10-Å periodicity only.

Sample Br1270 [(R = 0) I–S, 0% I]. Figure 11 shows a typical lattice-fringe image with layer spacings of 12–13 Å, consisting of smectite treated with L.R. White resin. Lattice fringes of smectite are anastomosing, curved, have variable contrast, and common layer terminations. The SAED pattern (inset, Figure 11) has only a small number of weak and very diffuse 001 reflections. Pore space is abundant. No illite or I–S-like fringes were interstratified with those of smectite. Packets with I1 lattice fringes were commonly observed, however, but separate from smectite packets. The sample is thus comprised of smectite free of illite-like layers, and separate I1 I–S.

https://doi.org/10.1346/CCMN.2001.0490204 Published online by Cambridge University Press

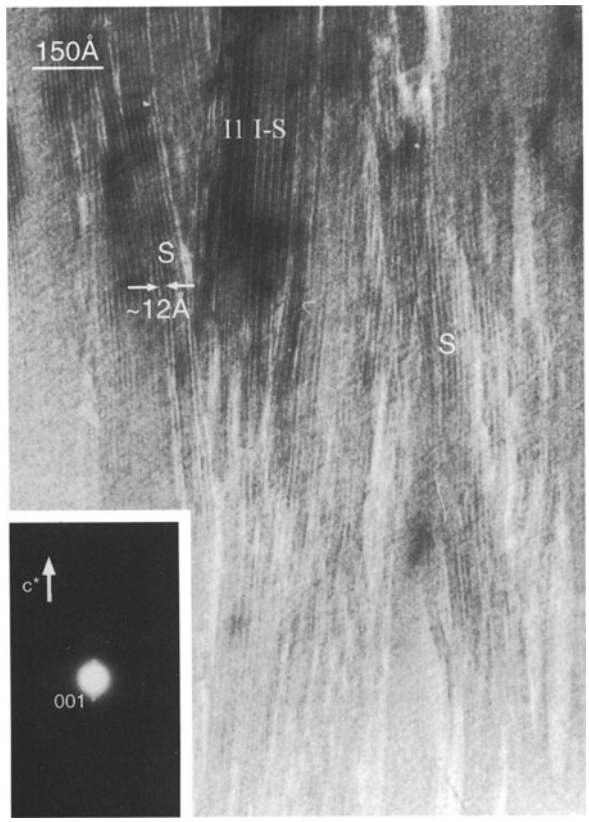

Figure 11. High-resolution TEM lattice-fringe image of sample Br1270. Almost all fringes correspond to smectite, having spacings of 12–13 Å, anastomosing orientations, and variable contrast. Layer terminations are common, and pore space is abundant. No fringes with 10-Å spacing occur interlayered with smectite. I1 I-S lattice fringes occur in separate, thin packets.

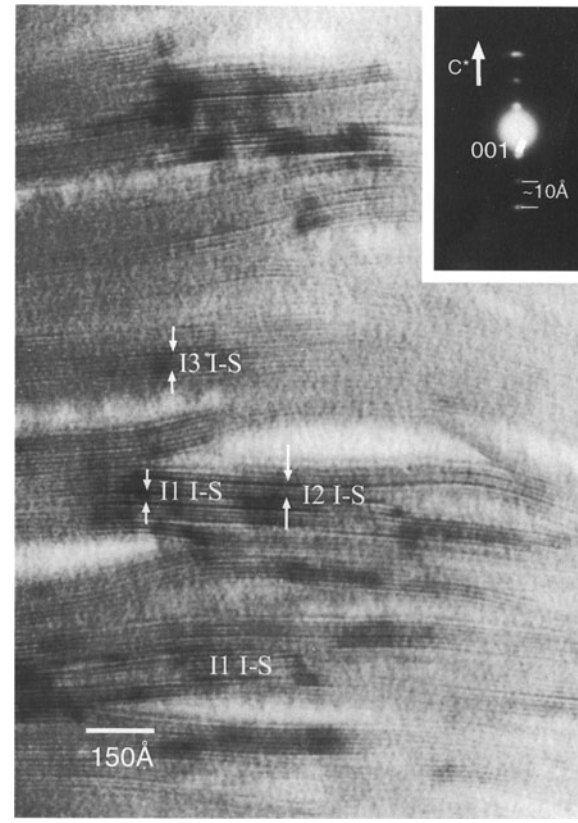

Figure 12. High-resolution TEM lattice-fringe image of sample Br1702. I1 I-S units dominate the sequence, with some randomly intercalated 12 and 13 units.

Sample Br1702 [(R = 1) I–S, 50% I]. Lattice-fringe images (Figure 12) are dominated by I1 sequences, with some I2 units and less common I3 units. No separate packets of smectite or illite were observed.

Sample Br1842 (100% I). Figure 13 shows lattice fringes occurring in well-defined individual packets. Such straight, parallel fringes, having relatively constant image contrast along layers, are typical of dioctahedral phyllosilicates having no expandable layers. Indeed, all fringe spacings are 10 Å, *i.e.,* no smectite-like fringes were observed, and layer terminations are rare. Individual packets are ~200–300 Å thick. Cross fringes were rarely observed, but they cut across entire packets when detected. No smectite or I–S was observed.

The SAED pattern (Figure 13, inset) shows well-defined 10-Å periodicity in non-00*l* reflections, corresponding to 1*M* polytypes. Some stacking disorder occurs, as indicated by diffuseness in non-00*l* reflections. Other packets give SAED patterns typical of $2M_1$ polytypism. A given packet is dominated by one or the other polytypic stacking sequence, with both types being intergrown. Similar intergrowths were observed by Lonker and Fitzgerald (1990) for samples from the Broadlands system. Packets of both polytypes are referred to as mica (see above).

AEM analyses

Table 2 shows average chemical formulae from AEM data involving concentration ratios, normalized to 22 oxygen atoms. All analyses were obtained after verifying, by TEM imaging, the identity of the clay. Because I–S interstratification usually involves different I*n* units, a given analysis of I–S is an average over such units, a slightly different composition being inferred to correspond to different values of *n*. The data of Table 2 do not show a regular trend because of reversals in the sequence of the proportions of illite-like layers down-core. However, Figure 14 shows that ^{IV}Si decreases, when plotted against the proportion of illite-like layers. This trend is expected for dioctahedral, interstratified clays, and was also observed by Tillick *et al.* (2001) for dioctahedral clays of the Golden Cross deposit.

To determine if compositional relations are related to the occurrence of the 1*M* polytype of mica relative

https://doi.org/10.1346/CCMN.2001.0490204 Published online by Cambridge University Press

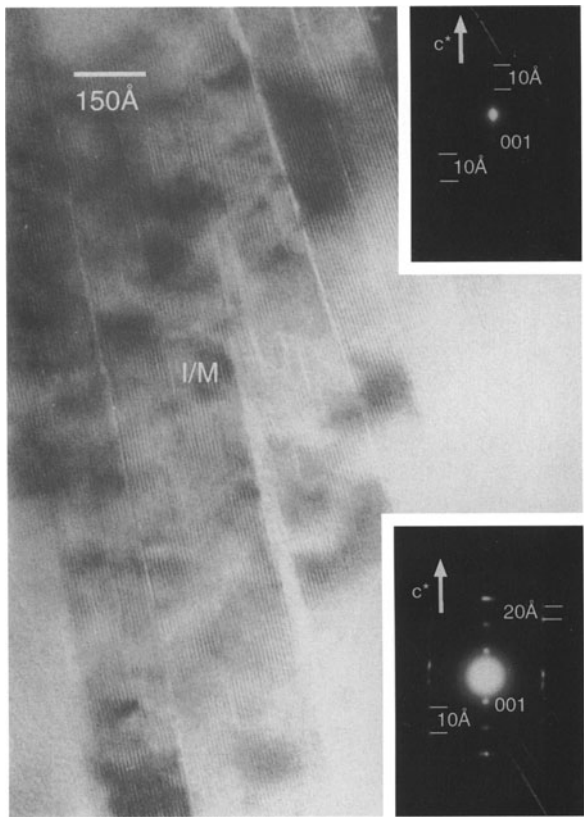

Figure 13. High-resolution TEM lattice-fringe image of sample Br1842. Well-defined individual packets of illite occur. Fringes are straight, parallel, have spacings of 10 Å, and have relatively constant image contrast. Packets are ~200–300 Å thick. The inset SAED patterns show well-defined 10-Å periodicity in 0*kl* reflections (upper inset), corresponding to 1*M* polytypism, and $2M_1$ polytypism (20-Å periodicity; lower inset). I/M = mica.

to the $2M_1$ polytype, analyses were obtained of packets where SAED analyses showed the dominance of one polytype. Formulae of each polytype are listed in Table 2. There are sharp differences in the analyses, those for the 1*M* polytype having much larger concentrations of ^{VI}Mg (and Fe + Mg).

DISCUSSION

Clay-mineral sequence

The overall sequence of clay minerals observed in the Broadlands-Ohaaki system is similar to those recognized as typical of sedimentary burial-metamorphic sequences in which smectite transforms to interstratified I–S to illite, although small-scale reversals occur. Several significant differences were observed in the samples of Broadlands-Ohaaki, as well as those described by Tillick *et al.* (2001). These involve (1) the absence of interstratification of smectite and illite in (R = 0) I–S, (2) a gap between I–S with high proportions of illite-like layers and illite, and (3) the presence of 1*M* polytypism.

Table 2. Average AEM chemical formulae[2] of Broadlands-Ohaaki dioctahedral clay minerals.

	Br533	Br693	Br836	Br1270	Br1702	Br1842 (1*M*)	Br1842 ($2M_1$)
Si	6.65	6.93	6.83	7.12	6.86	6.43	6.70
^{IV}Al	1.35	1.07	1.17	0.88	1.14	1.57	1.30
^{VI}Al	3.33	3.95	3.81	3.52	3.81	3.32	3.58
Fe^{2+}	0.07	0.14	0.14	0.46	0.06	0.31	0.05
Mg	0.71	n.d.	0.18	0.29	0.18	0.57	0.29
Mn	n.d.[1]	0.07	n.d.	n.d.	n.d.	0.06	0.01
Ca	0.06	n.d.	0.08	n.d.	0.34	0.04	0.03
Na	0.35	n.d.	n.d.	n.d.	0.33	n.d.	0.31
K	1.32	0.81	0.97	0.58	0.23	1.66	1.57

[1] n.d. = not-detected.
[2] Formulae are normalized to a total of 2 oxygen atoms, and are an average for each sample. Fe is assumed to be ferrous.

Smectite-I–S relation. It is generally accepted (*e.g.*, Środoń and Eberl, 1984) that there is a continuous sequence in interstratification in pelitic sediments between pure smectite and (R = 1) I–S (50% illite), with such intermediate materials designated as (R = 0) I–S, with <50% illite. This sequence strongly implies that a continuous series of transformations exists in which the proportion of illite-layers increases continuously.

The smectite samples observed in this study were from specimens which were identified as (R = 0) I–S by XRD. By TEM, however, no individual illite-like layers were identified randomly interstratified in smectite, *i.e.*, layers have spacings of 12–13 Å, typical of smectite treated with L.R. White resin. On the other hand, lattice fringes were observed with alternating contrast and ~21-Å periodicity of alternating illite- and smectite-like layers in (R = 1) I–S. Such units were clustered in sequences of four or six consecutive fringes. These data suggest that, at least for the samples of this study, there is a gap between smectite and I1 I–S where two clay minerals coexist rather than

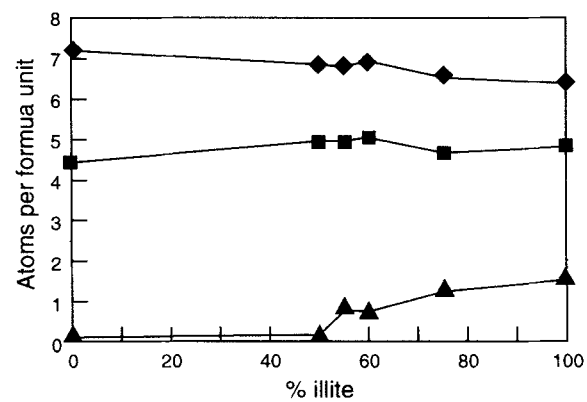

Figure 14. Plot of atoms pfu *versus* % illite layers. ◆: Si; ■: Al; ▲:K.

https://doi.org/10.1346/CCMN.2001.0490204 Published online by Cambridge University Press

occurring as random mixing of illite- and smectite-like layers.

Our observations of smectite-rich materials are similar to those of Dong *et al.* (1997) who emphasized the dominance of smectite, (R = 1) I–S and illite in diagenetic sequences. Those observations were of shales, however, and included samples from the classic Gulf Coast sequence. The Broadlands-Ohaaki data therefore imply that the lack of a continuum in R = 0 interstratification may be a common feature. Moreover, Dong *et al.* noted that such occurrences are required and predictable by the uniqueness of the (R = 1) I–S (50% illite) crystal structure. We caution that continuous sequences, which are favored by rapid crystallization at low temperatures, may also occur. Nevertheless, the relations described here show that the usually assumed, continuous sequence is absent in many sequences, including some where XRD data indicate a continuum. These conclusions are in partial accord with Bethke *et al.* (1986) for trends in I–S based on XRD data for shales, bentonites, and hydrothermal systems. They showed that although there is a continuous series of (R = 0) I–S from smectite through illite for shales, their data for hydrothermal systems implied that smectite was not a precursor to (R = 1) I–S. Although the Broadlands-Ohaaki and Golden Cross systems include smectite at lower grades, the implied gap for those systems between smectite and (R = 1) I–S is compatible with the data of Bethke *et al.*

Non-occurrence of illite-rich I–S. Golden Cross and Broadlands-Ohaaki samples identified as (R = 1) I–S by XRD display I–S sequences in lattice fringe images. Where XRD indicates the proportion of illite-like layers is ~50%, the layer sequences are dominated by I1 units, with random intercalation primarily of I2 units, and uncommon I3 units. As the proportion of illite-like layers determined by XRD increases, the proportion of I*n* units having $n > 1$ increases. A sample dominated by I2 units also has substantial numbers of I1 and I3 units, for example.

SAED patterns of I–S display the usual sequence of 00*l* reflections with *d* values which are submultiples of 10 Å. Even where layer sequences are dominated by I1 units, superperiodicity is generally not observed. For those samples where XRD data indicate there are ~50 ± 10% illite layers, however, and where TEM displays dominance of I1 units, a weak, diffuse 003 reflection (based on 20-Å superperiodicity) was commonly observed.

Sample GX4 of Tillick *et al.* (2001) is typical of illite-rich I–S. This material was expected to consist, or have dominant units, of I*n* with *n* equal to large numbers (dominant illite-like layers with random smectite-like layers). TEM images show that the sample is composed of packets of layers having 10-Å spacings (*i.e.*, illite) and separate packets with sequences of I–S, however. The I–S is comprised of a variety of I*n* units; $n = 1$ units are common, and sequences of as many as five or six I2 or I3 layers occur. The sample consists largely of separate illite and I–S, therefore, rather than only of illite with randomly interstratified smectite-like layers.

Bauluz *et al.* (2000) observed similar relations for a prograde sequence of I–S in metasediments, showing that as grade increased, the value of *n* of the dominant I*n* unit increased. In samples where $n = 3$ or 4 was dominant, discrete packets of illite with no or almost no smectite-like layers occurred. Similarly, Dong *et al.* (1997) observed, for Gulf Coast shales, I–S dominated by I1 units which coexists with separate, discrete packets of illite.

Only a small number of samples were examined by TEM in the Broadlands-Ohaaki and Golden Cross systems, so conclusions on the lack of completeness of a sequence of interstratified I–S to illite are tentative. However, observation of equivalent relations elsewhere, in samples of contrasting geological types, is supportive of such a relation. These observations imply that a gap, or at least paucity of illite-rich I–S relative to the end-members (R = 1) I–S and illite, is common. Such relations are predicted by the uniqueness (low free energy) of the Al-Si ordering of the R = 1 structure, in contrast to simple interlayering of smectite and illite layers, as reviewed by Dong *et al.* (1997).

Inoue *et al.* (1992) and Inoue (1995) concluded, from XRD data, that the smectite-to-illite sequence was continuous in hydrothermal systems. Ylagan *et al.* (1996) implied the same for hydrothermal alteration of silicic volcanic rocks, although Bauluz *et al.* (2000) concluded that an incomplete series exists based on TEM data. Christidis (1995) implied a continuous series for a hydrothermally altered bentonite, but noted that (R = 0) I–S and (R = 1) I–S coexisted in one sample. As noted above, Bethke *et al.* (1986) concluded that in hydrothermal systems, the I–S series begins with (R = 1) I–S, in contrast to shales where a continuum from smectite was implied. Those relations suggest direct crystallization of (R = 1) I–S from solution in hydrothermal systems. They also support the notion of uniqueness of the (R = 1) I–S structure, although Bethke *et al.* concluded that the I–S series is continuous between (R = 1) I–S and illite in hydrothermal systems. XRD data generally, but not always, imply completeness, whereas TEM data (see above) imply two gaps. Whether the different conclusions are both correct for different systems, is related to differences in sample preparation, or is a result of the inherent information acquired owing to the difference in wavelengths of the two methods, requires additional work.

Coexistence of more than one member of the illite-smectite sequence, as described for smectite plus (R

= 1) I–S, and (R = 1) I–S plus illite, may be interpreted, without textural information, as being related to overprinting by an event which modified the mineral assemblage of an earlier event (Inoue, pers. comm.). For TEM images obtained here and those for the Golden Cross mine, textures imply, but do not prove, that coexisting minerals formed at the same time, however. The coexisting clay minerals occur as intergrown, parallel packets, without preferential spatial distributions of either. Where multiple events are known to occur, packets of first-formed clay minerals commonly show alteration to a second, from the rim and proceeding inward, or along layers. We observed no along-layer transitions, however. Textures compatible with formation in the same event, and the absence of textures which reflect multiple events, are compelling evidence for simultaneous formation of the coexisting pairs of clay minerals. These relations are basic to an understanding of the processes of formation (below).

1M Polytypism. Illite in diagenetic environments typically displays an SAED pattern with diffuse and nonperiodic 0*kl* reflections indicating a high degree of stacking disorder, which is labeled $1M_d$ (Grubb *et al.,* 1991). Dong and Peacor (1996) reviewed the results of SAED patterns, concluding that the normal prograde sequence of polytypes in sedimentary sequences is $1M_d$ to $2M_1$, with no intermediate 1*M* polytype as commonly assumed. The $2M_1$ stacking relations were dominant where layers were coherently related even in material showing $1M_d$ SAED patterns. However, 1*M* polytypism was observed in the Potsdam sandstone (Reynolds and Thomson, 1993), in samples from the Silverton Caldera (Eberl *et al.,* 1987), and the Broadlands-Ohaaki geothermal field (Lonker and Fitzgerald, 1990).

SAED patterns of mica obtained from both Golden Cross and Broadlands-Ohaaki systems here and in Tillick *et al.* (2001) showed 1*M* polytypism (0*kl* reflections with $k \neq 3N$ have reflections with 10-Å periodicity). Unlike SAED patterns for mature mica, however, diffuseness also occurred parallel to c^* along all reciprocal lattice rows. Illite-rich I–S gave SAED patterns with weak 10-Å periodicity superimposed on the typical $1M_d$-like pattern, *i.e.,* even immature, disordered material tends to the 1*M*-like stacking sequence. This is in sharp contrast to the dominance of $2M_1$ stacking inferred for even immature Gulf Coast I–S.

Where the 1*M* polytype was observed in Broadlands-Ohaaki samples, however, it coexists with separate packets of the $2M_1$ polytype, similar to samples of Potsdam sandstone (Dong, pers. comm.) and samples from the Broadlands-Ohaaki geothermal system (Lonker and Fitzgerald, 1990; Dong, pers. comm.). To detect differences between the two types, AEM analyses were obtained for packets identified as to polytype. Compositions are different (Table 2). These data show that 1*M* material has a large ^{VI}Mg content. Although Mg is often accompanied by similar concentrations of Fe, the Fe content is not large in this case.

Such large Mg (and Fe) content has been correlated with formation at high pressure (Velde, 1965; Merriman and Peacor, 1999). It occurs in phengitic mica which has $2M_1$ polytypism, so there is no direct correlation between composition and polytypism. On the other hand, the 1*M* polytype is common to the celadonite group, dioctahedral micas which occur in volcanic rocks and whose net negative charge derives exclusively from Mg and Fe substitution in octahedral sites. The analyses of this study show that up to ~25% of octahedral cations are comprised of Mg and Fe, values which are large even by comparison with phengite from high-pressure environments. We therefore tentatively suggest that 1*M* polytypism observed in these studies is related to ordering of Mg (and Fe) on octahedral sites similar to celadonite. Additional composition data for 1*M* stacking sequences are necessary to verify this relation, however.

Layer stacking relations

SAED patterns of smectite displayed only diffuse low-order 00*l* reflections, semi-arcuate 0*kl* reflections, and both 0*kl* and *h*0*l* reflections in the same patterns. The latter indicates that turbostratic stacking occurs between most but not all layers. Limited coherency within I–S and smectite is demonstrated by weak nonperiodic 0*kl* reflections and by 4.5-Å cross-fringes spanning several 001 fringes. The thickness of such coherent layer sequences increases as the proportion of illite-like layers increases in a given sample. Guthrie and Reynolds (1998) noted that cross-fringes may be visible even where there are relative layer rotations $\leq 15°$ around c^*, and thus they may indicate either coherent or semi-coherent layer relations. In either case, however, the cross-fringes demonstrate that turbostratic stacking is not the only interlayer relation, and some layers have ordered relative orientations. Such materials are three-dimensional, albeit disordered crystals, rather than randomly interstratified, independent layers. Thus these materials are not collections of fundamental particles, by definition (Peacor, 1998).

Conditions of formation

Figure 3 shows that the general distribution of the sequence smectite to I–S to illite, as determined by XRD for the Broadlands-Ohaaki field, is generally consistent with measured well temperatures, *i.e.,* mica occurs at greatest depths and temperatures, and smectite at the lowest temperatures, but only for averaged data, however. As emphasized by Simmons and Browne (2000), there are significant exceptions to regular clay-mineral sequences as a function of temperature, *e.g.,* for samples studied herein from well Br7

in Figure 5b. The lack of a one-to-one relation between the state of the dioctahedral clays and temperature is consistent with Tillick *et al.* (2001) for the Golden Cross system, where heterogeneous clay mineral sequences reflect variable porosity and permeability controlled by fractures and rock textures. Similar heterogeneities were observed for the Broadlands-Ohaaki system (Simmons and Browne, 2000). The textures as observed by TEM are remarkable when compared to textures of clay-rich sediments, in having interpacket porosities estimated to be ≤25% of the total rock volume. As demonstrated experimentally by Whitney (1990), and as consistent with factors controlling reaction kinetics (Essene and Peacor, 1995), water/rock ratio is significant in determining reaction progress for the sequence smectite to I–S to illite. The distribution of clay minerals is thus seen to be primarily controlled by temperature, but with variations in the sequence mitigated by local heterogeneities in texture and structure, and thus by porosity and permeability (Simmons and Browne, 2000).

In summary, the Golden Cross samples show that crystallization occurred through a process of dissolution and crystallization (DC; Altaner and Ylagan, 1997) directly in pore space. TEM observations of Tillick *et al.* (2001) and here show homogeneous individual packets of one clay mineral (although more than one clay mineral may coexist as separate packets), and a very high proportion of pore space, as consistent with such a mechanism. Along-layer transitions were nearly non-existent, and larger-scale transitions involving packets were not observed. The presence of gaps in the series of interstratified I–S, between smectite and (R = 1) I–S and for large proportions of illite-like layers, provides compelling evidence for direct crystallization from fluids, rather than replacement of preexisting, lower-temperature clays.

The geothermal system was short-lived, ~150,000 to 500,000 y (Weissberg *et al.,* 1979), such that introduction of hydrothermal fluids and an elevation of the thermal gradient occurred relatively rapidly. This is consistent with Tillick *et al.* (2001) that clay minerals formed by direct crystallization from fluids, with reactants derived from original rocks, but is in contrast to the generally accepted notion of progressive "transformations" between clay minerals. All clay minerals are thus inferred to have formed simultaneously by crystallization from fluids as initially suggested by Browne and Ellis (1970), with components derived from similar original-rock reactants, the variations in clay mineral assemblages being a direct function of temperature as modified by the water/rock ratio.

The conditions are analogous to the Salton Sea system, where clay minerals are forming now through convecting hydrothermal fluids and an elevated geothermal gradient (G. Giorgetti, pers. comm.). The Salton Sea system is intermediate in some ways to the Golden Cross and Broadlands-Ohaaki systems, which involve hydrothermal alteration of volcanic rocks, and sedimentary systems such as Gulf Coast pelitic sediments where conditions are commonly assumed to correspond to burial metamorphism. In the "episodic" Salton Sea geothermal field, all clay minerals formed simultaneously. Dioctahedral clay minerals in Gulf Coast shales are usually visualized as having evolved with transformations occurring continuously as a function of time (Hower *et al.,* 1976). Bethke *et al.* (1986) noted that XRD data show that I-S sequences evolve along different pathways in hydrothermal systems and in shales, concluding that there was no evidence for a smectite precursor to ordered I-S in hydrothermal systems. In the systems studied herein, however, smectite is observed at the lowest temperatures. Whether or not an apparent smectite precursor is observed, XRD data imply a continuous sequence of clay minerals in both kinds of systems, at least from (R = 1) I-S to illite. Such a sequence is thus a necessary condition for time-dependent, sequential transformations, but it is not sufficient to prove they occurred. There is compelling geochemical evidence for episodic formation of clay minerals in Gulf Coast pelites (Morton, 1985; Ohr *et al.,* 1991), which are commonly taken as a "type" example of burial metamorphism. We do not infer that such sedimentary systems are necessarily entirely episodic in nature. Pevear (pers. comm.) has suggested that burial can occur so rapidly that it appears to be episodic on a geological time scale. We do suggest, however, that clay-mineral formation may not be time-dependent. Any systems with sequences of dioctahedral clay minerals may have been affected by some degree of episodic or time-dependent burial metamorphic processes. As noted by Inoue (pers. comm.), there may be more than one set of episodic changes, so that the textures of an earlier step are overprinted later. The terms "transformations" or "transitions" are often over-used, but non-continuous processes should also be considered, as they may be important mechanisms by which some, if not most, clay minerals form.

ACKNOWLEDGMENTS

We are indebted to B. Bauluz and L-S. Kao for valuable discussions and advice regarding TEM observations. C.E. Henderson is thanked for his kind help with the SEM and STEM. We are grateful to A. Inoue, G. Christides, S. Altaner, and S. Guggenheim for their constructive and helpful reviews. This work was supported by NSF grants EAR-94-18108 and EAR-98-14391 to D.R. Peacor, and the New Zealand Foundation for Research, Science and Technology (FRST). D.A. Tillick is grateful to the Australasian Institute of Mining and Metallurgy (AusIMM) and the Society of Economic Geologists (SEG) for financial support. The STEM was acquired under NSF grant EAR-87-08276 and the SEM under grant BSR-83-14092.

REFERENCES

Altaner, S.P. and Ylagen, R.F. (1997) Comparison of structure modes of mixed-layer illite/smectite and reaction mechanisms of smectite illitization. *Clays and Clay Minerals,* **45,** 517–533.

Bauluz, B., Peacor, D.R., and Lopez, J.M.G. (2000) TEM study of illitization in pelites from the Iberian Range, Spain: Layer-by-layer replacement? *Clays and Clay Minerals,* **48,** 374–384.

Bethke, C.M., Vergo, N., and Altaner, S.P. (1986) Pathways of smectite illitization. *Clays and Clay Minerals,* **34,** 125–135.

Browne, P.R.L. (1969) Sulfide mineralisation in a Broadlands geothermal drill hole, Taupo Volcanic Zone, New Zealand. *Economic Geology,* **64,** 156–159.

Browne, P.R.L. (1971) *Petrological logs of Broadlands drillholes BR1 to BR 25.* New Zealand Geological Survey Report, **52,** 86 pp.

Browne, P.R.L. (1973) The geology, mineralogy and geothermometry of the Broadlands geothermal field, Taupo Volcanic Zone, New Zealand. Ph.D. thesis, Victoria University of Wellington, New Zealand, 153 pp.

Browne, P.R.L. and Ellis, A.J. (1970) The Ohaaki-Broadlands geothermal area, New Zealand: Mineralogy and related geochemistry. *American Journal of Science,* **269,** 97–131.

Christidis, G.E. (1995) Mechanism of illitization of bentonites in the geothermal field of Milos Island, Greece: Evidence based on mineralogy, chemistry, particle thickness and morphology. *Clays and Clay Minerals,* **43,** 569–585.

Dong, H. and Peacor, D.R. (1996) TEM observations of coherent stacking relations in smectite, I/S and illite of shales: Evidence for MacEwan crystallites and dominance of $2M_1$ polytypism. *Clays and Clay Minerals,* **44,** 257–275.

Dong, H., Peacor, D.R., and Freed, R.L. (1997) Phase relations among smectite, R = 1 illite-smectite, and illite. *American Mineralogist,* **82,** 379–391.

Eberl, D.D., Środoń, J., Lee, M., Nadeau, P.H., and Northrop, H.R. (1987) Sericite from the Silverton caldera, Colorado: Correlation among structure, composition, origin, and particle thickness. *American Mineralogist,* **72,** 914–934.

Eslinger, E.V. and Savin, S.M. (1973) Mineralogy and oxygen isotope geochemistry of the hydrothermally altered rocks of the Ohaaki-Broadlands, New Zealand geothermal area. *American Journal of Science,* **273,** 240–267.

Essene, E.J. and Peacor, D.R. (1995) Clay mineral thermometry—a critical perspective. *Clays and Clay Minerals,* **43,** 540–553.

Grindley, G.W. and Browne, P.R.L. (1968) *Subsurface Geology of the Broadlands Geothermal Field.* New Zealand Geological Survey Report **34,** 41 pp.

Grubb, S.M.B., Peacor, D.R., and Jiang, W.-T. (1991) Transmission electron microscope observation of illite polytypism. *Clays and Clay Minerals,* **39,** 540–550.

Guthrie, G.D., Jr. and Veblen, D.R. (1989) High-resolution transmission electron microscopy of mixed-layer illite/smectite: Computer simulation. *Clays and Clay Minerals,* **37,** 1–11.

Guthrie, G.D., Jr. and Reynolds, R.C., Jr. (1998) A coherent TEM- and XRD-description of mixed-layer illite/smectite. *Canadian Mineralogist,* **36,** 1421–1434.

Hedenquist, J.W. (1986) Geothermal systems of the Taupo Volcanic Zone: Their characteristics and relation to volcanism and mineralisation. In *Late Cenozoic Volcanism in New Zealand,* I.E.M. Smith, ed., Royal Society of New Zealand Bulletin 23, 134–168.

Hedenquist, J.W. (1990) The thermal and geochemical structure of the Broadlands-Ohaaki geothermal system. *Geothermics,* **19,** 151–185.

Hedenquist, J.W. and Stewart, M.K. (1985) Natural CO_2-rich steam-heated waters at Broadlands, New Zealand: Their chemistry, distribution and corrosive nature. *Proceedings of the Geothermal Resources Council Annual Meeting Transactions,* **9,** 245–250.

Henley, R.W., Hedenquist, J.W., and Roberts, P.J., eds. (1986) *Guide to the Active Epithermal Systems and Precious Metal Deposits of New Zealand. Monograph Series Mineral Deposits, Volume 26,* Gebruder Borntraeger, Berlin, 211 pp.

Hower, J., Eslinger, E.V., Hower, M.E., and Perry, E.A. (1976) Mechanism of burial metamorphism of argillaceous sediments: Mineralogical and chemical evidence. *Geological Society of America Bulletin,* **87,** 725–737.

Inoue, A. (1995) Formation of clay minerals in hydrothermal environments. In *Origin and Mineralogy of Clays,* B. Velde, ed., Springer-Verlag, Berlin, 268–329.

Inoue, A. and Utada, M. (1983) Further investigations of a conversion series of dioctahedral mica/smectites in the Shinzan hydrothermal alteration area, Northeast Japan. *Clays and Clay Minerals,* **31,** 401–412.

Inoue, A., Utada, M., and Wakita, K. (1992) Smectite-to-illite conversion in natural hydrothermal systems. *Applied Clay Science,* **7,** 131–145.

Lonker, S.W. and Fitzgerald, J.D. (1990) Formation of coexisting 1M and 2M polytypes in illite from an active hydrothermal system. *American Mineralogist,* **75,** 1282–1289.

Masuda, H., O'Neil, J.R., Jiang, W.-T., and Peacor, D.R. (1996) Relation between interlayer composition of authigenic smectite, mineral assemblages, I/S reaction rate and fluid composition in silicic ash of the Nankai Trough. *Clays and Clay Minerals,* **44,** 443–459.

Merriman, R.J. and Peacor, D.R. (1999) Very low grade metapelites: Mineralogy, microfabrics and measuring reaction progress. In *Low-Grade Metamorphism,* M. Frey and D. Robinson, eds., Blackwell Science, Oxford, 10–60.

Morton, J.P. (1985) Rb-Sr evidence for punctuated illite/smectite diagenesis in the Oligocene Frio Formation, Texas Gulf Coast. *Geological Society of America Bulletin,* **96,** 67–76.

Ohr, M., Halliday, A.N., and Peacor, D.R. (1991) Sr and Nd isotopic evidence for punctuated clay diagenesis, Texas Gulf Coast. *Earth and Planetary Science Letters,* **105,** 110–126.

Peacor, D.R. (1998) Implications of TEM data for the concept of fundamental particles. *Canadian Mineralogist,* **36,** 1397–1408.

Reynolds, R.C., Jr. and Thomson, C.H. (1993) Illite from the Potsdam sandstone of New York: A probable noncentrosymmetric mica structure. *Clays and Clay Minerals,* **41,** 66–72.

Simmons, S.F. and Browne, P.R.L. (1997) Saline fluid inclusions in sphalerite from the Broadlands-Ohaaki geothermal system: A coincidental trapping of fluids boiled to dryness. *Economic Geology,* **92,** 485–489.

Simmons, S.F. and Browne, P.R.L. (2000) Hydrothermal minerals and precious metals in the Broadlands-Ohaaki geothermal system: Implications for understanding low-sulfidation epithermal environments. *Economic Geology,* **95,** 971–999.

Simmons, S.F. and Christenson, B.W. (1994) Origins of calcite in a boiling geothermal system. *American Journal of Science,* **294,** 361–400.

Simmons, S.F., Browne, P.R.L., and Brathwaite, R. (1992) Active and extinct hydrothermal systems of the North Island, New Zealand. *Society of Economic Geologists Field Guide Series 15,* 121 pp.

Środoń, J., and Eberl, D.D. (1984) Illite. In *Micas, Reviews in Mineralogy, volume 13,* P.H. Ribbe, ed., Mineralogical Society of America, Washington, D.C., 495–544.

Tillick, D.A., Peacor, D.R., and Mauk, J.L. (2001) Genesis of dioctahedral phyllosilicates during hydrothermal alteration of volcanic rocks: I. The Golden Cross Epithermal Ore Deposit, New Zealand. *Clays and Clay Minerals,* **49,**

Veblen, D.R., Guthrie, G.D., Jr., Livi, K.J.T., and Reynolds, R.C., Jr. (1990) High-resolution transmission electron microscopy and electron diffraction of mixed-layer illite/smectite: experimental results. *Clays and Clay Minerals,* **38,** 1–13.

Velde, B. (1965) Phengite micas: Synthesis, stability and natural occurences. *Americal Journal of Science,* **263,** 886–913.

Weissberg, B.G., Browne, P.R.L., and Seward, T.M. (1979) Ore metals in active geothermal systems: In *Geochemistry of Hydrothermal Ore Deposits, 2nd edition,* H.L. Barnes, ed., J. Wiley and Sons, New York, 738–780.

Whitney, G. (1990) Role of water in the smectite-to-illite reaction. *Clays and Clay Minerals,* **38,** 343–350.

Ylagan, R.F., Altaner, S.P., and Pozzuoli, A. (1996) Hydrothermal alteration of a rhyolitic hyaloclastite from Ponza Island, Italy. *Journal of Volcanology and Geothermal Research,* **74,** 215–231.

Yau Y.-C., Peacor, D.R., and Essene, E.J. (1987) Smectite to illite reaction in Salton Sea shales: A transmission and analytical electron microscopy study. *Journal of Sedimentary Petrology,* **57,** 335–342.

E-mail of corresponding author: drpeacor@umich.edu

(Received 22 February 2000; accepted 20 September 2000; Ms. 429; A.E. Stephen Altaner)